POLITECNICO
MILANO 1863

SCUOLA DI INGEGNERIA INDUSTRIALE
E DELL'INFORMAZIONE

Executive Summary of the Thesis

Development of Experimental and Computational Non-Destructive Assay techniques for the Safeguards of Lead-Cooled Reactor fuel

Laurea Magistrale in Nuclear Engineering - Ingegneria Nucleare

Author: Alessandro Brovelli

Advisor: Prof. Antonio Cammi

Co-advisor: Marc Looman, Paolo Peerani, Nicola Cavallini, and Andrea Favalli

Academic year: 2025-2026

1. Introduction

Computational methods are widely employed in Non-Destructive Assay (NDA) to support measurements and develop detector systems for nuclear safeguards applications. Neutron and photon transport can be simulated by solving the linear Boltzmann transport equation [1], either stochastically with the Monte Carlo method [2, 3], where each particle history is simulated, or with deterministic solvers, by inverting the linear system arising from the discretization of the phase space and the integro-differential operator. Experimental validation of these methods is crucial to ensure their reliability under real operational conditions.

Due to the high dimensionality of the problem, classical deterministic methods suffer from the *curse of dimensionality* [4], meaning that computational and memory costs scale exponentially with the dimensionality of the phase space. For this reason, Monte Carlo methods have so far been the preferred simulation technique for NDA and safeguards applications.

This work, carried out during the Scientific Traineeship Program at the Joint Research Centre (JRC) of the European Commission in Ispra, presents research and applications of NDA numerical methods for the safeguards of advanced nuclear energy systems.

The main effort focused on the design of a Passive Neutron Coincidence Collar (PNCC) [5] for the verification of ALFRED (Advanced Lead Fast Reactor European Demonstrator) fresh fuel assemblies. In this reactor concept, the use of highly plutonium-enriched mixed oxide (MOX) fuel results in significant spontaneous neutron emission through spontaneous fission (SF) and (α, n) reactions, which can be exploited to quantify the plutonium content via coincidence counting measurements.

A model of the PNCC was developed in MCNP-PTA [6], an extension of MCNP [7] developed at JRC Ispra for coincidence counting detector simulations. The model was experimentally validated using ^{252}Cf and plutonium oxide (PuO_2) samples and then applied to study plutonium quantification and diversion scenarios for ALFRED fuel assemblies.

In parallel, advanced deterministic numerical methods were investigated with the goal of reducing the computational cost of transport simulations using the Tensor Train format [8, 9] to represent high-dimensional data structures in a low-dimensional subspace. Preliminary results

for a simple model of the multi-group (MG) neutron transport equation are presented.
Together, these efforts constitute the basis for the research and development of fast and reliable experimental and computational methods to support the application of NDA to next-generation nuclear reactors.

2. ALFRED fuel assembly design

ALFRED is a reactor concept for a 125 MWe pool-type lead-cooled fast reactor, aimed at demonstrating the technological readiness and feasibility of lead technology for European Generation IV nuclear systems [10, 11].
Its design features hexagonal fuel assemblies [12, 13], each containing 126 fuel pins. The fuel is a highly plutonium-enriched MOX fuel $(Pu_yU_{1-y})O_2$, where the plutonium weight fraction relative to total heavy metal is 21.7% and 27.8% for the inner and outer enrichment zones, respectively [14]. A single fuel assembly can contain up to 13 kg of reactor-grade plutonium, which exceeds the IAEA definition of a significant quantity (SQ) of 8 kg [15]. The spontaneous neutron yield from combined spontaneous fission (SF) and (α, n) reactions is approximately $7-9 \times 10^6$ n/s, which is significant and enables the use of passive assay techniques without an external neutron interrogation source.

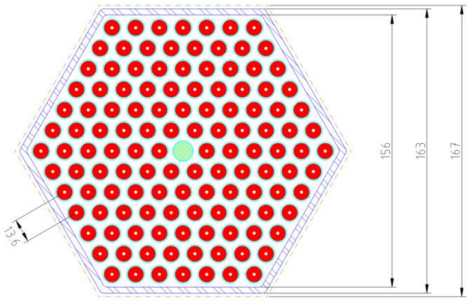

Figure 1: ALFRED fuel assembly design. Dimensions in mm [13]

3. Design of a PNCC and modeling in MCNP-PTA

A JCC-71 neutron coincidence collar [16] in passive mode was selected, given it is a standard model routinely utilized in IAEA safeguards inspections. ^{3}He tubes used were Reuter-Stokes model RS-P4-0813-101 [17] with fill gas pressure of 5.35 atm and composition: 20.935 wt% ^{3}He, 69.323 wt% Ar and 9.742 wt% CH_4. Each of the four High Density Polyethilene (HDPE, $\rho = 0.965$ g/cm^3) bank contains six detector tubes, for a total of 24. The collar cavity was set at 17×23.5 cm. The shift register used was N2000 by ANTECH [18] with predelay set at 4.5 μs and gate width of 64 μs. For the experimental campaigns, a single pulse-shaping amplifier was connected to each detector bank, hence each had input signal from 6 ^{3}He tubes.
The detector geometry and materials composition was reproduced in MCNP-PTA (Pulse Train Analysis), an extension of the MCNP code developed and benchmarked at the JRC Ispra. PTA allows to compute the SF and (α, n) yields given the source cell isotopic composition, as well as simulating the front end electronics response and shift register counting logic to extract coincidence counting observables: singles (S) and especially doubles (D) count rates which are proportional to the fissile content of the item.

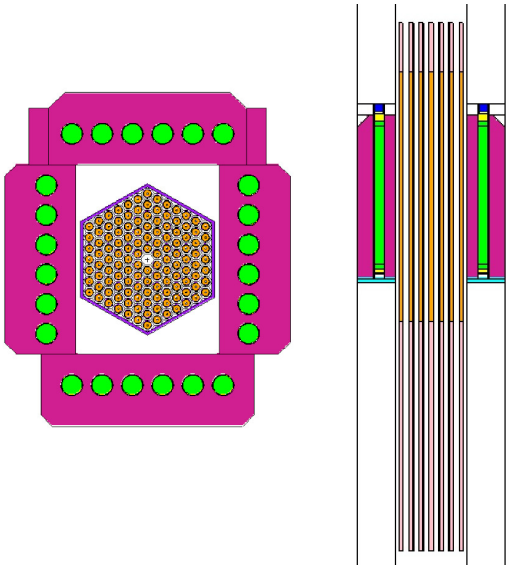

Figure 2: MCNP-PTA geometry of the PNCC with the ALFERD fuel assembly

4. Experimental validation of the Monte Carlo model

To verify the accuracy and reliability of the MCNP-PTA model of the PNCC, a series of experimental campaigns were carried out to gather data to compare with simulations that represented the same scenarios. The percent devi-

ation of Monte Carlo (C_m) counts compared to experimental ones (C_e) is presented, defined as

$$\text{Dev.}(\%) = 100 \cdot \left| 1 - \frac{C_m}{C_e} \right| \quad (1)$$

The uncertainties propagate as

$$\sigma_{\text{Dev}} = 100 \frac{C_m}{C_e} \sqrt{\left(\frac{\sigma_m}{C_m}\right)^2 + \left(\frac{\sigma_e}{C_e}\right)^2} \quad (2)$$

A first measurement set with a ^{252}Cf source (Q2-988, yield 2.160×10^5 n/s) was conducted, positioning the source capsule at different positions within the collar cavity. The singles detection efficiency was found to vary between 0.162 in the center of the cavity and 0.170 towards the HDPE walls. Due to unaccounted experimental and modeling uncertainties, deviations between simulations and measurements remained within 2% for singles and 4.5% for doubles.
A second measurement with a ^{252}Cf source (Q2-987, yield 3.217×10^4 n/s) was conducted on an elevated structure built to avoid backscattering effects from the laboratory floor. The source capsule was set at the center of the collar cavity. Results showed very precise agreement for this scenario.

	Dev. [%]
S $[s^{-1}]$	0.161 $\pm$0.027
D $[s^{-1}]$	0.781 $\pm$ 0.178

Table 1: Comparison between experimental and Monte Carlo results for the measurement with the Q2-987 source. NPS 1e7 and measurement time 2d 22h 14m.

Subsequent measurements used PuO_2 samples in order to mimic the spontaneous neutron emission properties of a MOX fuel. The samples used were CBNM NRM 271 [19], a set of 4 samples labeled Pu61, Pu70, Pu84 and Pu93 where the number is approximately the wt% content of ^{239}Pu. Two measurements were run, one with just the Pu61 sample in the center of the cavity and one with all 4 samples, each shifted 3 cm from the center towards one of the collar walls. For the PuO_2 samples deviations within 1% for the singles and 2% for the doubles were found.

	Dev. (%)
Pu61	
S $[s^{-1}]$	0.762 $\pm$ 0.063
D $[s^{-1}]$	1.789 $\pm$ 0.466
Full set	
S $[s^{-1}]$	0.671 $\pm$ 0.046
D $[s^{-1}]$	1.369 $\pm$ 0.467

Table 2: Comparison between experimental and Monte Carlo results for CBNM. NPS 5×10^6 for Pu61 and 1×10^7 for the full se, while measurement times were 1h 10m and 4h 56m respectively.

5. Extension of the validated model to the simulation of the ALFRED fuel assembly verification

The experiments showed that the MCNP-PTA model of the PNCC can reproduce the detector response to various neutron sources with good agreement. In particular, the campaign with the PuO_2 samples demonstrated that PTA is able to correctly compute both SF and (α, n) yields, which is crucial for simulating MOX fuels. Since a reference measurement with a mock-up fuel assembly was not available, the uncertainty observed in the doubles count rate for the PuO_2 comparison was included as an additional model bias when reproducing experimental observations. A conservative systematic uncertainty of 2% ($f = 0.02$) was therefore introduced for the doubles count rates, and the total uncertainty was computed as

$$\sigma = \sqrt{(\sigma_D)^2 + (fD)^2} \quad (3)$$

where D and σ_D are the simulated doubles count rate and its Monte Carlo uncertainty, respectively. Each reported value x in this section is therefore expressed as

$$x \pm \sigma_x \ (\pm\sigma) \quad (4)$$

where σ_x is the statistical (Monte Carlo) uncertainty and σ is the total uncertainty including the 2% systematic contribution.

5.1. Calibration curve for plutonium quantification

Since the MOX fuel under investigation has a fixed isotopic composition (reactor grade Pu with 27% ^{240}Pu [20]), the effective linear density of ^{240}Pu (m^{eff}_{240} [g/cm]) can be used to establish a relationship with the simulated doubles count rate. It is defined as [21]

$$m^{eff}_{240} = 2.52, m_{238} + m_{240} + 1.68, m_{242} \quad (5)$$

where m_i denotes the linear density of the corresponding Pu isotope, and the coefficients are proportional to the spontaneous fission yield and second factorial moment of the neutron multiplicity distribution relative to ^{240}Pu.

Five different plutonium enrichments were simulated, varying linearly from 21.7% to 28.7% Pu/(U+Pu), resulting in m^{eff}_{240} values ranging from 66.19 to 84.86 g/cm.

To limit count rates and mitigate dead-time effects, a 1 mm thick cadmium liner was inserted into the collar cavity to suppress thermal-induced multiplication (fast mode). This reduced the doubles count rate by a factor of approximately 1.7. However, when using a single amplifier for six tubes, the doubles count rate reached saturation for all simulated enrichments due to signal pile-up and OR-logic losses. Therefore, the effect of increasing the number of amplifiers was investigated, up to one per detector tube (24 in total).

The configuration with 24 amplifiers provided the best linearity and response quality and was therefore used to derive the calibration curve via linear least-squares regression on the simulated doubles count rates.

5.2. Diversion scenarios

To benchmark diversion scenarios, a reference calculation was performed for the full fuel assembly at 21.7% Pu enrichment, corresponding to an effective linear ^{240}Pu density of 66.19 g/cm and a doubles count rate of 83907 ± 359 (± 1678) counts per second. This value originates from a total neutron yield (spontaneous fission plus (α, n)) of 7.56×10^6 n/s. Deviations from this reference are reported according to Eqs˙ 1 and 2.

All simulations were performed with 5×10^8 source particles (NPS). This corresponds to 66 seconds of physical emission time for the assembly. This equivalence provides a useful interpretation of the simulation as a physical measurement duration. For this class of scenarios, a detection threshold can be defined in terms of the normalized deviation

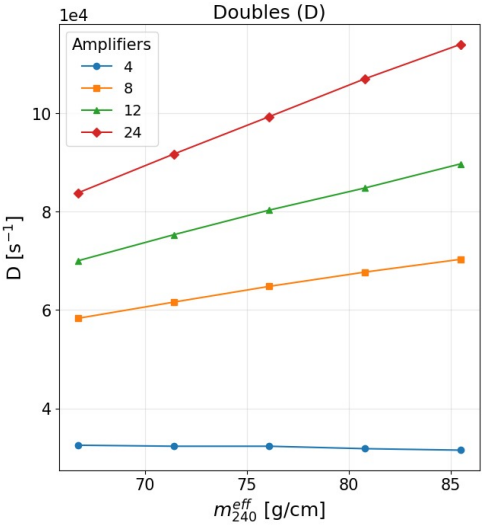

Figure 3: Calibration curves for various amplifiers configurations. It can be noted how the response to a higher enrichment gets better by increasing the number of amplifiers. NPS 5×10^8 for each point.

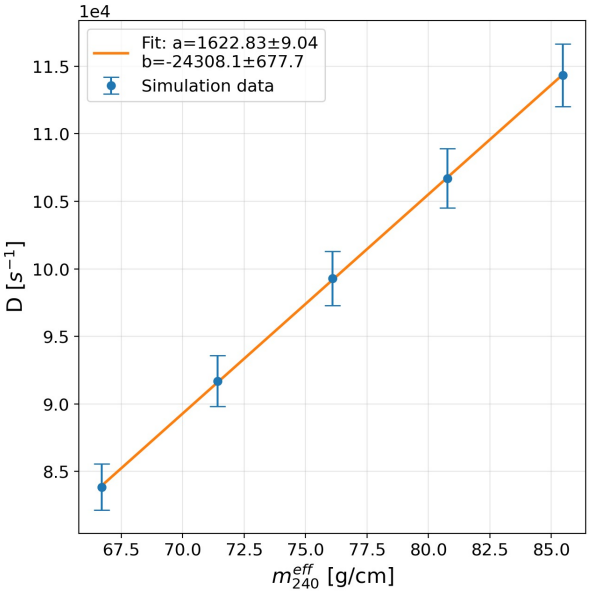

Figure 4: Calibration curve for the ALFRED fuel assembly varying Pu/(Pu+U) enrichment. The simulation data, which included the systematic 2% uncertainty, was fitted by a weighted least-squares regression of the form $D = (a \pm \sigma_a) m^{eff}_{240} + (b \pm \sigma_b)$. NPS 5×10^8 for each point.

$$\frac{\mathrm{Dev}(\cdot)}{\sigma_{\mathrm{Dev}}} = 2 - 3 \tag{6}$$

which indicates reliable detectability of a given defect.

5.2.1 Single pin removal

The sensitivity of the model to a single-pin defect was investigated. This corresponds to a reduction of approximately 0.8% in fuel mass. The fuel assembly was divided into hexagonal rings labeled from 1 (inner) to 6 (outer) as in Figure 5. A single pin removal from each ring was simulated.

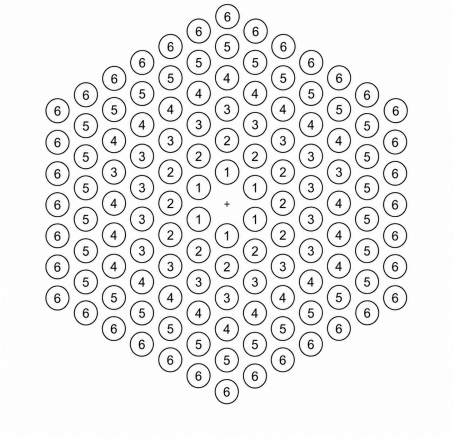

Figure 5: Six rings division of the ALFRED fuel assembly. Each pin is identified by its ring index 1 to 6

On average, the simulated doubles count rate decreased by 1.76 ± 0.56 (± 2.83)%, corresponding to $\mathrm{Dev}(D)/\sigma_{\mathrm{Dev}} = 3.14$ (0.62). Considering only statistical uncertainty, the system would appear sensitive enough to detect a single-pin removal from all positions, since the deviation exceeds the Monte Carlo uncertainty. However, once the additional systematic uncertainty is included, the significance decreases, indicating that a single-pin removal cannot be reliably detected under the assumed measurement time and model bias.

5.2.2 Multiple pins replaced with steel

Here, first 18 and then 6 fuel pins were replaced with steel pins of identical geometry. For these scenarios, the expected values of m_{240}^{eff} are 56.73 and 63.04 g/cm, respectively. The replaced pins were located at different positions within the fuel assembly, identified by the ring index.
For the 18-pin replacement scenario, corresponding to a 14.3% reduction in plutonium content, two configurations were studied: replacement in the inner rings (1–2) and in the outermost ring (6). In both cases, a clear reduction in the detected signal was observed, leading to a significant underestimation of the plutonium content with respect to the reference assembly. The results are summarized in Table 3. The average normalized deviation was $\mathrm{Dev}(m_{240}^{eff})/\sigma_{\mathrm{Dev}} = 17.07$ (9.44), indicating that this defect configuration is clearly detectable. The average deviation from the expected m_{240}^{eff} was 1.59 ± 0.97 (± 1.76).

Ring	$\mathrm{Dev}(D)$ [%]	$\mathrm{Dev}(m_{240}^{eff})$ [%]
1,2	20.93 ± 0.30 (± 1.63)	15.59 ± 0.82 (± 1.48)
6	17.44 ± 0.40 (± 1.72)	12.86 ± 0.85 (± 1.54)

Table 3: Deviations for the 18 replaced pins scenario relative to the reference case of the full fuel assembly

To further assess system sensitivity, a second set of simulations was performed with 6 replaced pins, corresponding to a 4.76% reduction in m_{240}^{eff}. Pins were removed at the vertices of rings 1, 3, and 6. The results are reported in Table 4. In this case, the average normalized deviation decreased to $\mathrm{Dev}(m_{240}^{eff})/\sigma_{\mathrm{Dev}} = 3.84$ (2.02), indicating that the defect is close to the detection threshold for the selected measurement time. Nevertheless, the reconstructed plutonium content remains close to the expected value, with an average deviation of 1.31 ± 0.94 (± 1.78).

Ring	$\mathrm{Dev}(D)$ [%]	$\mathrm{Dev}(m_{240}^{eff})$ [%]
1	5.32 ± 0.56 (± 1.90)	3.40 ± 0.93 (± 1.75)
3	6.44 ± 0.48 (± 1.87)	4.28 ± 0.90 (± 1.71)
6	4.63 ± 0.52 (± 1.90)	2.86 ± 0.92 (± 1.75)

Table 4: Deviations for the 6 replaced pins scenario relative to the reference case of the full fuel assembly.

6. Tensor Train for deterministic particle transport

So far in this work, Monte Carlo simulations have been chosen since they are the standard in NDA for simulating particle transport in complex 3D geometries, heterogeneous materials, and detailed interaction physics. However, Monte Carlo can be computationally expensive when a high number of particle histories (NPS) is required to achieve sufficient statistical precision, and it cannot naturally treat time-dependent problems.

In recent years, deterministic particle transport has gained renewed interest thanks to high-performance computing and advances in low-rank tensor methods such as the Tensor Train (TT) format [8, 9]. In this format, high-dimensional functions and discrete operators are represented as sets of 3- and 4-dimensional tensors, respectively, called TT cores. The TT decomposition of a d-dimensional function evaluated on a grid can be written as

$$\psi(x_1,\dots,x_d) = \sum_{\alpha_1=1}^{r_1} \cdots \sum_{\alpha_{d-1}=1}^{r_{d-1}} G^{(1)}(x_1,\alpha_1) G^{(2)}(\alpha_1,x_2,\alpha_2)\dots G^{(d)}(\alpha_{d-1},x_d) \tag{7}$$

where r_i for $i = 0,\dots,d$ (with $r_0 = r_d = 1$) are the TT ranks and $G^{(i)}$ are the TT cores. Let n denote the maximum number of discretization points among the variables x_i, and r the maximum TT rank. While a full tensor representation scales as $\mathcal{O}(n^d)$ in memory, the TT representation scales as $\mathcal{O}(dnr^2)$. This highlights the memory savings, and the compression ratio is defined as the ratio between the number of elements in the TT representation and that of the full tensor.

Many physical PDE operators can be expressed in tensor-product form, where basis functions and grids admit separable representations, allowing tensor decompositions to be efficiently exploited.

The solution of the resulting multilinear system in TT format is enabled by the AMEn (Alternating Minimal Energy) solver [22], which iteratively sweeps through the TT cores and solves reduced local problems at each step.

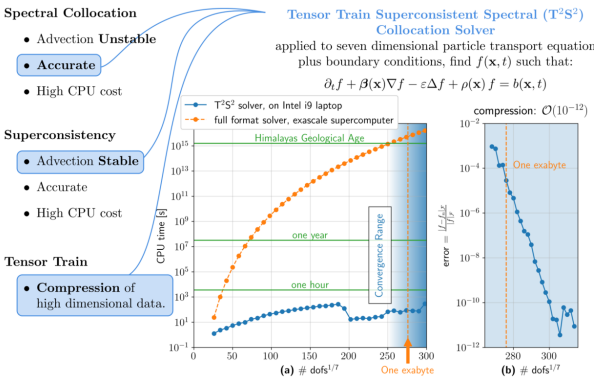

Figure 6: Key components of the T²S² solver. (a) Illustrates the compression capabilities, which enables real time solution of a seven-dimensional problem. The same problem with a number of degrees of freedoms (dofs) per dimension resulting in one exabite of memory required to store the full solution tensor runs in less than 1 hour on a Intel i9 laptop, compared to millions of years on a exascale supercomputer (supposed to run at 2.7 exaFLOPS). (b) Shows the convergence behaviour in which the error decreases exponentially to $\mathcal{O}(10^{-11})$. [23]

A major breakthrough in these numerical techniques was recently achieved at JRC Ispra with the development of the T²S² (Tensor Train Spectral Superconsistent) solver for the time-dependent advection–diffusion–reaction equation [23]. Numerical experiments reported errors as low as $\mathcal{O}(10^{-11})$, while maintaining compression ratios on the order of $\mathcal{O}(10^{-10})$.

6.1. Preliminary results for a neutron transport model

Following these advances, a finite-element solver for the neutron transport equation in TT format is being developed. Preliminary results for the multi-group, time-dependent equation in slab geometry are presented:

$$\left(\frac{1}{v_g}\frac{\partial}{\partial t} + \mu\frac{\partial}{\partial x} + \Sigma_{tg}\right)\psi_g(x,\mu,t) = \\ = \sum_{g'=1}^{G}\int_{-1}^{1}\Sigma_{s,g'\to g}(\mu',\mu),\psi_{g'}(x,\mu',t),d\mu' \\ + f_g(x,\mu,t) \tag{8}$$

where Σ_{tg} is the total cross section for group g,

$\Sigma_{s,g'\to g}(\mu',\mu)$ is the multi-group scattering differential cross section, v_g is the neutron group velocity, and f_g is an external source term. Energy groups are ordered in decreasing energy, so that $g = 1$ corresponds to the highest energy group and $g = G$ to the lowest. The spatial domain is a slab of length L, while $\mu \in [-1, 1]$ is the direction cosine relative to the x-axis. This results in a four-dimensional problem in space, angle, energy group, and time.

A discontinuous Galerkin (DG) finite element method was used with polynomial order p in each spatial cell. Angular discretization was performed using discrete ordinates (S_N). The time derivative was treated using a backward Euler scheme in matrix form, meaning that time was included as an additional tensor dimension and all time steps were solved simultaneously using AMEn.

A rank-one separable manufactured solution was proposed:

$$\begin{aligned}&\psi_g(x,\mu,t) = E_g \sin\left(\frac{\pi x}{L}\right)\\&(a_0P_0(\mu) + a_1P_1(\mu) + a_2P_2(\mu))\\&\left(1 - e^{-\alpha t}\right)\end{aligned} \tag{9}$$

where P_ℓ are Legendre polynomials of degree ℓ. The corresponding source term $f_g(x,\mu,t)$ was obtained by substitution into Eq. (8).

Let A denote the discrete operator arising from the numerical scheme, and let Ψ and F be the solution and source tensors, respectively. The computational grid consisted of $N_s = 500$ spatial cells with polynomial order $p = 1$, giving $\text{dof}_s = N_s(p+1) = 1000$, $N_a = 100$ angular directions, $G = 10$ energy groups, and $N_t = 1000$ time steps.

With this configuration, the TT representation of the operator required approximately 40 MB of memory, compared to about 64 GB for the full dense representation, corresponding to a compression of approximately $\mathcal{O}(10^{-12})$.

AMEn (implemented in the TorchTT Python library [24]) was used to solve the linear system $A\Psi = F$, achieving a relative residual $\rho = |A\Psi - F|/|F|$ (Frobenius norm) of 10^{-5} within three sweeps. The solution tensor Ψ in TT format occupied only 155 kB of memory with TT ranks $r = 7$, corresponding to a compression ratio of approximately $\mathcal{O}(10^{-5})$. The resulting L^2 error in the spatial domain (for fixed g, μ, and t) was on the order of 10^{-4}–10^{-5}.

7. Conclusions

This work developed and experimentally validated a passive neutron coincidence methodology for safeguards verification of ALFRED fresh MOX fuel assemblies and explored low-rank deterministic transport methods for accelerating future NDA simulations.

The MCNP-PTA model of the PNCC was successfully validated through experimental campaigns with ^{252}Cf and PuO_2 samples. The results demonstrated the capability of the code to accurately compute neutron yields and reproduce the detector response under different measurement conditions.

The validated model was then extended to the simulation of fresh ALFRED fuel assemblies, enabling the construction of a calibration curve relating the doubles count rate to the effective ^{240}Pu linear density. To manage the high spontaneous neutron emission of the fuel, optimal operating conditions were identified using a 1 mm cadmium liner and a configuration with 24 independent amplifiers. Since experimental measurements with a representative ALFRED fuel assembly mock-up were not available, an additional systematic model uncertainty of 2%, derived from the PuO_2 validation campaign, was included in all simulations. Each simulation was performed with 5×10^8 source particles, corresponding to an equivalent physical measurement time of approximately 66 s.

Diversion scenarios were investigated to evaluate the sensitivity of the system to defects in the fuel assembly. Under the selected measurement conditions and uncertainty assumptions, the removal of a single fuel pin could not be reliably detected regardless of its position within the assembly. Larger defects, such as the replacement of 18 fuel pins with steel pins, produced deviations well above the detection threshold and were therefore clearly identifiable. The scenario with 6 replaced pins was found to be close to the selected detection limit.

Further improvements in detection capability could be achieved through longer measurement times, which would reduce statistical uncertainty, and through a more accurate quantification of model bias via dedicated experimental validation. Additional simulations involv-

ing more diversified diversion scenarios would provide a broader assessment of system performance. Although developed for ALFRED, the methodology can be naturally extended to other MOX fuel concepts characterized by high spontaneous neutron emission.
In parallel, preliminary numerical experiments on deterministic neutron transport demonstrated the potential of the Tensor Train format to solve the time-dependent multi-group neutron transport equation with substantial reductions in memory requirements and computational cost. For the simplified slab-geometry model considered, accurate solutions were obtained while maintaining strong compression of both operators and solution tensors.
Future work should include a systematic convergence study to assess numerical accuracy under mesh refinement and increasing discretization resolution, together with extensions toward more realistic multidimensional transport problems and ultimately full 3D geometries.

References

[1] J. J. Duderstadt and W. R. Martin. *Transport Theory*. Wiley, 1979.

[2] J. M. Hammersley and D. C. Handscomb. *Monte Carlo Methods*. Wiley, 1964.

[3] I. Lux and L. Koblinger. *Monte Carlo Methods: Particle Transport Methods*. CRC Press, 1991.

[4] R. E. Bellman. *Dynamic Programming*. Princeton University Press, 1957.

[5] H. O. Menlove. Passive/active coincidence collar for plutonium measurement. *Los Alamos National Laboratory*, (LA-9288-MS), 1982.

[6] M. Looman, P. Peerani, and H. Tagziria. Monte carlo simulation of neutron counters for safeguards applications. *Nuclear Instruments and Methods in Physics Research A*, 598:542–550, 2009.

[7] J. F. Briesmeister. MCNP—a general monte carlo N-particle transport code. Technical Report LA-13709-M, Los Alamos National Laboratory, 2000.

[8] I. V. Oseledets. Tensor-train decomposition. *SIAM J. Sci. Comput.*, 33:2295–2317, 2011.

[9] P. Gelß. *The Tensor Train Format and Its Applications*. PhD thesis, TU Berlin, 2017.

[10] Generation IV International Forum. A technology roadmap for generation IV nuclear energy systems, 2002. GIF-002-00.

[11] A. Alemberti et al. The status of the ALFRED project. In *IAEA FR21 Conference*, Beijing, China, 2021. IAEA.

[12] G. Grasso et al. The core design of ALFRED, a demonstrator for european lead-cooled reactors. *Nuclear Engineering and Design*, 278:287–301, 2014.

[13] G. Grasso et al. Improved core design for the ALFRED core. In *ICAPP 2019*, Juanles-Pins, France, 2019.

[14] L. Luzzi, A. Cammi, V. Di Marcello, S. Lorenzi, D. Pizzocri, and P. Van Uffelen. Application of the TRANSURANUS code for the fuel pin design process of the ALFRED reactor. *Nuclear Engineering and Design*, 277:173–187, 2014.

[15] International Atomic Energy Agency. *IAEA Safeguards Glossary*. Number 3 in International Nuclear Verification Series. IAEA, Vienna, Austria, 2002.

[16] A. T. Simone, S. Croft, J.P. Hayward, and L.G. Worral. Using the JCC-71 neutron coincidence collar as a benchmark for detector characterization with PTR-32 list mode data acquisition. *Nuclear Instruments and Methods in Physics Research A*, 908:24–34, 2018.

[17] Reuter-Stokes, Baker Hughes. *Helium-3 Position Sensitive Proportional Counter Datasheet*, 2025.

[18] ANTECH. *Universal Neutron Counter Datasheet*, 2023.

[19] R. J. Friar and T. E. Sampson. Plutonium isotopic abundance measurements on CBNM NRM 271. Technical Report LA-12309-MS, Los Alamos National Laboratory, 1991.

[20] V. Sobolev, E. Malambu, and H.A. Abderrahim. Design of a fuel element for a lead-cooled fast reactor. *Journal of Nuclear Materials*, 385:392–399, 2009.

[21] W. H. Geist, P. A. Santi, and M. T. Swinhoe. *Nondestructive Assay of Nuclear Materials for Safeguards and Security*. Springer, 2 edition, 2024.

[22] S. V. Dolgov and D. V. Savostyanov. Alternating minimal energy methods. *SIAM J. Sci. Comput.*, 2013.

[23] N. Cavallini, G. Manzini, D. Funaro, and A. Favalli. A fast, accurate and oscillation-free spectral collocation solver for high-dimensional transport problems. *Scientific Reports*, 16(1):498, 2026.

[24] G. Ion. torchTT: A PyTorch-based tensor-train toolbox. *Journal of Open Source Software (JOSS)*, 11, 2026.